Research Square

Preprints are preliminary reports that have not undergone peer review.
They should not be considered conclusive, used to inform clinical practice,
or referenced by the media as validated information.

A Modified First-Order Kinetic Model for Re-Evaluating Petroleum Hydrocarbon Biodegradation Under Bioaugmentation and Bio-stimulation

yusuf . o. l momoh

loymoly@aol.com

University of Port Harcourt

Research Article

Keywords: Bioremediation kinetics, Hindrance coefficient, Bioaugmentation, Biostimulation, Total petroleum hydrocarbons, Model selection

Posted Date: November 13th, 2026

DOI: https://doi.org/10.21203/rs.3.rs-11490590/v1

License: This work is licensed under a Creative Commons Attribution 4.0 International License.
Read Full License

Additional Declarations: No competing interests reported.

A Modified First-Order Kinetic Model for Re-Evaluating Petroleum Hydrocarbon Biodegradation Under Bioaugmentation and Bio-stimulation

Abstract

First-order kinetics is widely used to compare soil bioremediation treatments but assumes a constant degradation rate. This study developed a hindrance-modified first-order kinetic model (HM-FOKM), applied it to a published pilot-scale dataset, and examined how the fitting method affects the parameters behind remediation forecasts. The HM-FOKM lets the first-order rate constant decline linearly with time and reduces to first-order kinetics when the hindrance coefficient $H = 0$. Petroleum hydrocarbon and degrader data for natural attenuation, bioaugmentation, biostimulation and combined treatment of crude-oil-contaminated soil (10 weekly samples) were digitised from Yaman (2020). Both models were fitted directly to concentration–time data and compared using R^2, AICc, an F test and profile-likelihood intervals. The rate–concentration procedure behind the published constants was reconstructed and tested. The HM-FOKM fitted better in all treatments (R^2 0.976–0.986 vs 0.905–0.931; ΔAICc 9.8–12.8), with H positive and significant. Published constants, from a rate–concentration regression biased even for first-order data, were 1.5–3.4 times too large. Degradation slowed while degraders were still increasing, indicating substrate-side limitation. Nutrients raised the initial rate 2.7-fold; bioaugmentation alone had little effect. Projected maximum removal was 38–73%, reached at 9.2–10.8 weeks, versus 90% implied by first-order kinetics. Estimating rate constants from linearised or rate-based plots introduces systematic error when degradation slows, and the error propagates into remediation forecasts. Parameters should be fitted directly to concentration–time data. The HM-FOKM, a nested extension of first-order kinetics, separates initial rate from slowdown and better estimates achievable removal.

Keywords Bioremediation kinetics · Hindrance coefficient · Bioaugmentation · Biostimulation · Total petroleum hydrocarbons · Model selection

I Introduction

Crude oil is a complex mixture of aliphatic hydrocarbons, polycyclic aromatic hydrocarbons (PAHs), resins and asphaltenes. The aliphatic fraction (alkanes and cycloalkanes) is generally the most readily biodegraded, whereas higher-molecular-weight PAHs, resins and asphaltenes are more persistent and more toxic to microbial communities (Leahy and Colwell 1990; Varjani 2017; Koshlaf and Ball 2017). When this mixture is released into soil from pipelines, refineries or storage facilities it becomes one of the most widespread sources of terrestrial contamination, and biological treatment is usually the least costly remediation option (Lee et al. 2024; Mekonnen et al. 2024; Mohanta et al. 2024; Alao et al. 2025).

Three strategies are routinely compared. Natural attenuation relies on the indigenous microbial community; biostimulation supplies nitrogen and phosphorus to relieve nutrient limitation; and bioaugmentation introduces hydrocarbon-degrading microorganisms (Margesin and Schinner 2001; Chaîneau et al. 2005; Nikolopoulou et al. 2013; Wu et al. 2016; Koshlaf and Ball 2017). Relative performance varies with soil and contaminant: biostimulation has outperformed bioaugmentation in some studies (Kauppi et al. 2011; Sayara et al. 2011; Abed et al. 2014), while the largest removals have been reported when the two were combined (Mancera-López et al. 2008; Taccari et al. 2012; Suja et al. 2014; Cerqueira et al. 2014; Polyak et al. 2018; Safdari et al. 2018).

These comparisons rest almost entirely on kinetic parameters. First-order kinetics, $C(t) = C_0 e^{-kt}$, remains the default because it has a single parameter and yields a half-life directly (Alexander 1999; Rončević et al. 2005; Komilis et al. 2010; Agamuthu et al. 2013; Nwankwegu et al. 2016; Liu et al. 2018). Its central assumption—that the fraction of hydrocarbon removed per unit time is constant—is frequently violated by total petroleum hydrocarbon (TPH) data. Removal is typically rapid at first and then slows as the labile fraction is exhausted, the residue weathers, sorption reduces bioavailability and nutrients are depleted (Scow et al. 1986; Alexander 1999; Ros et al. 2010; Jiang et al. 2016; Ramadass et al. 2018). A single constant fitted across both phases therefore averages early and late behaviour and can misrepresent both the true rate and the time required to reach a regulatory target (Adair et al. 2010).

More mechanistic alternatives exist. Monod and Michaelis–Menten formulations link rate to substrate concentration and biomass (Simkins and Alexander 1984; Bekins et al. 1998; Rittmann and McCarty 2001; Ostendorf et al. 2007), but they require biomass measurements, a yield coefficient and at least two kinetic constants—information that short, sparsely sampled soil time series rarely supply. Empirical second-order models have described TPH removal more accurately than first-order kinetics in several amended soils (Sarkar et al. 2005; Nwankwegu et al. 2016; Ritoré et al. 2025, 2026), and modified growth-type models can capture lag and plateau phases (Momoh 2025). A simpler route is to retain the first-order structure while allowing the specific rate itself to vary with time (Odermatt 1997). In the present work the specific degradation rate is permitted to decline linearly, $k(t) = K - Ht$, so that integration of $\mathrm{d}C/\mathrm{d}t = -k(t)C$ produces the Hindrance-Modified First-Order Kinetic Model (HM-FOKM). Written in terms of the fraction of TPH removed,

$$B(t) = 1 - \exp\left(-Kt + \frac{H}{2}t^2\right), \qquad (1)$$

where K(week^{-1}) is the initial specific rate and H(week^{-2}) is a hindrance index. Positive H indicates progressive deceleration, negative H acceleration, and $H = 0$ recovers classical first-order kinetics exactly. The two models are therefore nested, and the data themselves can decide whether the additional parameter is required.

Because an extra parameter almost always improves residual fit, formal comparison must penalise complexity. For nested models fitted to the same observations the corrected Akaike information criterion (AICc) and the extra-sum-of-squares F test are standard (Bates and Watts 1988; Hurvich and Tsai 1989; Burnham and Anderson 2002). A profile-likelihood confidence interval for H further shows whether the data constrain the parameter away from zero (Venzon and Moolgavkar 1988; Raue et al. 2009). Such tests are most decisive when sampling is frequent and prolonged enough for any change in rate to become visible.

Yaman (2020) supplies a suitable data set. Four 0.4 m³ pilot-scale tanks of freshly crude-oil-contaminated soil (initial TPH 1674 mg kg^{-1}) were operated under natural attenuation (NA), combined bioaugmentation and biostimulation (BA+BS), bioaugmentation alone (BA) and biostimulation alone (BS). TPH and total hydrocarbon-degrading bacteria were measured weekly for 63 days (ten sampling occasions per treatment). Final removals were 35 % (NA), 74 % (BA+BS), 41 % (BA) and 66 % (BS). The author fitted first-order and Monod models and concluded that the Monod formulation described the data better. The reported first-order constants (0.0159–0.0419 d^{-1}), however, were obtained from rate–concentration plots rather than from the concentration–time series themselves. When reapplied to those series they predict day-63 concentrations of 119–615 mg kg^{-1}, against measured values of 430–1088 mg kg^{-1}. Whether the degradation rate itself changed over the 63 days was not examined.

The present study develops the HM-FOKM, applies it to the Yaman (2020) data and compares it with classical first-order kinetics. The objectives were to: (i) derive the HM-FOKM from first-order kinetics; (ii) reconstruct the TPH and degrader time series by digitisation and verify them against the values reported in the original text; (iii) fit both models to each treatment by nonlinear least squares; (iv) compare the models using R^2, AICc, the F test and a profile-likelihood interval for H; (v) reconstruct and test the rate–concentration procedure used to obtain the published rate constants; and (vi) relate the fitted parameters to the degrader counts and to the choice of treatment and monitoring duration.

2 Model development

2.1 Biodegradability and classical first-order kinetics

Biodegradability is defined as the fraction of contaminant removed:

$$B(t) = 1 - \frac{C(t)}{C_0} \quad (2)$$

where C_0 and $C(t)$ are the initial and current TPH concentrations (mg kg^{-1} dry soil). Under first-order kinetics with a constant rate constant k,

$$\frac{dB}{dt} = k\,(1 - B) \quad (3)$$

which integrates, with $B(0) = 0$, to

$$B(t) = 1 - \exp(-kt) \quad (4)$$

2.2 The hindrance-modified first-order kinetic model

The HM-FOKM relaxes the constant-k assumption by letting k depend on the concentration I of inhibitory by-products that accumulate during degradation. If I is produced at a rate p and removed, for example by aeration or volatilisation during mixing, at a rate v, then

$$\frac{dI}{dt} = p - v,\; I(t) = I_0 + (p - v)\,t \quad (5)$$

If the rate constant falls linearly with inhibitor concentration, $k = k_0 - \alpha I$, where α is the inhibition sensitivity, then

$$k(t) = K - Ht,\; K = k_0 - \alpha I_0,\; H = \alpha\,(p - v) \quad (6)$$

Substituting Eq. (6) into Eq. (3), with k replaced by $k(t)$, and integrating from $B(0) = 0$ gives the operative equation:

$$B(t) = 1 - \exp\left(-Kt + \frac{H}{2}t^2\right) \quad (7)$$

K is the initial specific degradation rate (week^{-1}) and H is the hindrance coefficient (week^{-2}). $H = 0$ recovers first-order kinetics exactly; $H > 0$, when by-product production outpaces removal, gives a decelerating trajectory; and $H < 0$ gives acceleration. Because the two fitted parameters lump four mechanistic quantities (k_0, α, I_0 and $p - v$), they describe the trajectory rather than identify a single process. In the Yaman (2020) tanks, daily mixing for aeration in tanks 2–4 is one possible removal process; tank 1 was not mixed.

2.3 Derived quantities

Three quantities follow from Eq. (7): the time at which degradation stops, the maximum biodegradability, and the time needed to reach a given removal.

Transition time. Differentiating Eq. (7) gives the removal rate

$$\frac{dB}{dt} = (K - Ht)\ \exp\left(-Kt + \frac{H}{2}t^2\right) = k(t)\left(1 - B(t)\right) \quad (8)$$

Because $1 - B(t) > 0$, the rate falls to zero only when $k(t) = K - Ht = 0$. For $H > 0$ this occurs at the transition time

$$t_{\text{trans}} = \frac{K}{H} \quad (9)$$

Before t_{trans} the rate is positive and B rises; after t_{trans} Eq. (7) would give a negative rate, that is, re-formation of contaminant. Because the model is not intended to describe this, B is held at its value at t_{trans} thereafter. For $H \leq 0$ the rate never reaches zero and no transition time exists.

Projected biodegradability. Substituting $t = K/H$ into the exponent of Eq. (7) gives

$$-K\left(\frac{K}{H}\right) + \frac{H}{2}\left(\frac{K}{H}\right)^2 = -\frac{K^2}{H} + \frac{K^2}{2H} = -\frac{K^2}{2H} \quad (10)$$

so the maximum, or projected, biodegradability is

$$B_{\text{proj}} = 1 - \exp\left(-\frac{K^2}{2H}\right) \quad (11)$$

B_{proj} is the largest fraction of TPH the HM-FOKM expects to be removed under the conditions that produced K and H. Under first-order kinetics ($H = 0$) it equals 1.

Time to a target removal. The time t_x at which a fraction x of the TPH has been removed ($x = 0.5$ for t_{50}, 0.9 for t_{90}) is found by setting $B(t_x) = x$ in Eq. (7):

$$1 - x = \exp\left(-Kt_x + \frac{H}{2}t_x^2\right) \ \Rightarrow\ \frac{H}{2}t_x^2 - Kt_x + \ln\left(\frac{1}{1-x}\right) = 0 \quad (12)$$

This quadratic in t_x has the roots $\left[K \pm \sqrt{K^2 - 2H\ln\left(1/(1-x)\right)}\right]/H$. The smaller root is the one reached before t_{trans} and is the physically meaningful solution:

$$t_x = \frac{K - \sqrt{K^2 - 2H\ln\left(\frac{1}{1-x}\right)}}{H},\ x = 0.5 \text{ or } 0.9 \quad (13)$$

A real solution exists only if $K^2 \geq 2H\ln[1/(1-x)]$, which, from Eq. (11), is the same as $B_{\mathrm{proj}} \geq x$. If $B_{\mathrm{proj}} < x$, the rate falls to zero before the target is reached and t_x is undefined. As $H \to 0$, Eq. (13) tends to the first-order result

$$t_x = \frac{1}{k}\ln\left(\frac{1}{1-x}\right),\ t_{50} = \frac{\ln 2}{k},\ t_{90} = \frac{\ln 10}{k} \quad (14)$$

which always exists because first-order removal continues indefinitely.

2.4 Assumptions

The derivation rests on four simplifying assumptions: the soil in each tank is treated as a single, well-mixed compartment; the rate constant declines linearly with inhibitor concentration; p and v are constant over the fitting window; and the hydrocarbon mixture behaves as a single pool. These are reasonable for the early-to-mid remediation window before the readily degradable fraction is exhausted, but they are not expected to hold indefinitely. The model should therefore not be extrapolated far beyond the observed 63 days without independent validation.

3 Materials and methods

3.1 Data source

TPH and microbial data were taken from Yaman (2020), a pilot-scale study of crude-oil-contaminated soil in four high-density polyethylene tanks (100 × 100 × 40 cm, 0.4 m^3 of soil each). Clean soil was spiked with 1 L of crude oil per tank, giving an initial TPH (C_{10}–C_{40}) of 1674 ± 9.25 mg kg^{-1}, and soil moisture was kept at 25% or more with tap water. The four treatments were:

I. **Tank 1, natural attenuation (NA):** no inoculum or nutrients, not mixed;

II. **Tank 2, bioaugmentation plus biostimulation (BA+BS):** microbial inoculum (dominated by *Alcanivorax*) and NH_4Cl and KH_2PO_4 to a C:N:P ratio of 100:5:1;

III. **Tank 3, bioaugmentation (BA):** inoculum only;

IV. **Tank 4, biostimulation (BS):** nutrients only.

Tanks 2–4 were aerated by daily mixing. TPH and total hydrocarbon-degrading bacteria (CFU g^{-1}) were measured at the start and weekly for 63 days, giving ten sampling times per treatment (0, 7, 14, …, 63 days). The original paper reports these time series only as figures (Figures 2 and 4 of Yaman 2020), as treatment means without error bars, although each treatment was run in triplicate.

Both figures were digitised from the 300 dpi images embedded in the published PDF. The axes were calibrated by least squares on the gridlines (maximum residual 1.8 pixels, about 6 mg kg^{-1}, for TPH), and each data point was taken as the centre of its marker, an approach that gives reliable values when the axes are carefully calibrated (Drevon et al. 2017); overlapping markers were separated using each marker's measured size. At day 0 all four TPH markers overlap, so the reported initial value of 1674 mg kg^{-1} was used for every tank. The digitised day-63 TPH values agreed with those stated in the text within 1.1%

(NA 1086 vs 1088 mg kg^{-1}; BA+BS 427 vs 430; BA 988 vs 988; BS 563 vs 569 mg kg^{-1}, the last two from the reported 41% and 66% removals). The digitised data are given in Supplementary Tables S1 and S2, and the digitised points are shown over the original images in Supplementary Fig. S1.

TPH concentrations were converted to biodegradability with Eq. (2), using $C_0 = 1674$ mg kg^{-1}, and time was converted from days to weeks ($t =$ day$/7$). Each treatment therefore has $n = 10$ points from 0 to 9 weeks. Because only means are available, the means were fitted.

3.2 Model fitting

The first-order model (Eq. 4) and the HM-FOKM (Eq. 7) were fitted to $B(t)$ for each treatment by nonlinear least squares (Bates and Watts 1988; Escuder-Gilabert et al. 2019), minimising the residual sum of squares

$$SS_{\mathrm{res}} = \sum_{i=1}^{n} \left(B_i - \hat{B}_i\right)^2 \quad (15)$$

where B_i is the observed and $\hat{B}_i$ the predicted biodegradability. A bounded trust-region algorithm was started from several initial values to avoid local minima, with $k, K > 0$ and $-2 \le H \le 2$ week^{-2}. The first-order rate constants reported by Yaman (2020) were converted from day^{-1} to week^{-1} for reference (Table 1). Because they were derived from rate–concentration plots rather than fitted to B(t), they were not included in the goodness-of-fit comparison (Table 2, Figure 1) and the procedure used to obtain them is examined separately (Section 3.4). Calculations used Python 3 with NumPy and SciPy.

The HM-FOKM can equally be written for the TPH concentration, $C_t = C_0 \exp(-Kt + Ht^2/2)$, and the first-order model as $C_t = C_0 \exp(-kt)$. Because C_0 was fixed at the measured value, $B = 1 - C/C_0$ is a linear transformation of C, so fitting C_t by nonlinear regression gives the same estimates of k, K and H, the same R^2, ΔAICc and F, and the same profile-likelihood intervals as fitting $B(t)$. This was confirmed numerically (differences in the estimates below 10^{-9}). Only the RMSE scales with C_0 (24–51 mg kg^{-1} for the HM-FOKM and 53–105 mg kg^{-1} for first-order kinetics), together with the absolute AICc values. Results are therefore reported for $B(t)$, which places all treatments on a common 0–1 scale.

3.3 Goodness of fit and model comparison

Goodness of fit was measured by the coefficient of determination and the root-mean-square error:

$$R^2 = 1 - \frac{SS_{\mathrm{res}}}{\sum_{i=1}^{n}(B_i - \bar{B})^2} \quad (16)$$

$$\mathrm{RMSE} = \sqrt{\frac{SS_{\mathrm{res}}}{n}} \quad (17)$$

where $\bar{B}$ is the mean observed biodegradability. The two models were compared using the corrected Akaike information criterion (Hurvich and Tsai 1989; Burnham and Anderson 2002),

$$\mathrm{AICc} = n \ln\left(\frac{SS_{\mathrm{res}}}{n}\right) + 2q + \frac{2q(q+1)}{n-q-1} \quad (18)$$

where q is the number of fitted parameters (1 for first-order, 2 for the HM-FOKM). $\Delta\mathrm{AICc} = \mathrm{AICc}(\text{first-order}) - \mathrm{AICc}(\text{HM-FOKM})$, so positive values favour the HM-FOKM; differences greater than 4 and 10 were taken as strong and very strong support for the model with the lower AICc (Burnham and Anderson 2002).

Because the models are nested, the extra-sum-of-squares F test was also applied (Bates and Watts 1988):

$$F = \frac{SS_{\mathrm{res,FO}} - SS_{\mathrm{res,HM}}}{SS_{\mathrm{res,HM}}/(n-2)} \quad (19)$$

which is compared with $F(1,\ n-2)$ at the 0.05 level ($F_{0.05} = 5.32$ for $n = 10$). Finally, a 95% profile-likelihood confidence interval for H was computed by fixing H at successive values, refitting K and finding the values at which the residual sum of squares reached

$$SS_{\mathrm{res,HM}}\left[1 + \frac{F_{0.05}(1, n-2)}{n-2}\right] \quad (20)$$

(Venzon and Moolgavkar 1988; Raue et al. 2009). An interval that excludes zero indicates that the data support a non-zero hindrance coefficient.

3.4 Rate-based estimation used by Yaman (2020)

Yaman (2020) estimated the first-order constants from the differential form of the rate law rather than from its integrated form. With reaction order $n = 1$, Eq. (1) of that paper is

$$r = -\frac{dC}{dt} = kC \quad (21)$$

where r is the TPH removal rate (mg kg^{-1} d^{-1}). The rate was not measured directly. Reconstructing Figure 5 of Yaman (2020) from the digitised data shows that it was calculated as the average removal rate since the start of treatment,

$$\overline{r}_i = \frac{C_0 - C_i}{t_i}, \quad i = 1, \ldots, 9 \quad (22)$$

with t_i in days, and that the point at C_0 was assigned the first-week rate $\overline{r}_1$, giving ten points per treatment. A straight line with an intercept was then fitted to $\overline{r}_i$ against C_i by ordinary least squares,

$$\overline{r}_i = a + kC_i \quad (23)$$

and its slope was reported as k, together with the R^2 of the regression. The intercept a was not reported. Equation (23) differs from Eq. (21) in two respects. First, it has a second parameter, so its R^2 measures the fit of a two-parameter line, not of $r = kC$. Second, it describes the average rate since day 0, not the instantaneous rate $-dC/dt$. A non-zero intercept also means that the fitted relationship is not first-order: for $a < 0$ the rate reaches zero while TPH remains (at $C = -a/k$), and for $a > 0$ removal would continue at $C = 0$.

The procedure is also not consistent with first-order kinetics itself. For exact first-order data, $C = C_0\exp(-kt)$, so $t = \ln(C_0/C)/k$ and Eq. (22) becomes

$$\overline{r} = \frac{C_0 - C}{t} = k\,\frac{C_0 - C}{\ln(C_0/C)} \quad (24)$$

The fraction on the right is the logarithmic mean of C_0 and C, which lies between C and C_0 and is close to their arithmetic mean. The average rate is therefore approximately $kC_0/2 + (k/2)C$, and a line fitted by Eq. (23) has a slope of about $k/2$ and a positive intercept of about $kC_0/2$, even when degradation is exactly first-order. To quantify this bias for the present data, Eqs. (22) and (23) were applied to the exact first-order curve of each treatment (Eq. 4 with the fitted k) and to its fitted HM-FOKM curve (Eq. 7), both sampled at the measurement times.

The standard first-order approach used in this study (Section 3.2) is different again. It fits the integrated rate law, Eq. (4), directly to $B(t)$, so its single parameter k is chosen to reproduce the measured concentrations over time, and its R^2 (Eq. 16) is computed on $B(t)$. The HM-FOKM (Eq. 7) is fitted in the same way.

To compare the fitted first-order model and the HM-FOKM on the basis used by Yaman (2020), both were also evaluated in rate space. Two observed rates were used: the average rate of Eq. (22) and the weekly rate

$$r_i = \frac{C_{i-1} - C_i}{\Delta t}, \quad \Delta t = 7\ \mathrm{d} \quad (25)$$

The corresponding rates predicted by each model were calculated from its predicted biodegradability $\hat{B}(t)$:

$$\hat{\overline{r}}_i = \frac{C_0\,\hat{B}(t_i)}{t_i}, \qquad \hat{r}_i = \frac{C_0[\hat{B}(t_i) - \hat{B}(t_{i-1})]}{\Delta t} \quad (26)$$

where $\hat{B}$ was given by Eq. (4) with the fitted k or by Eq. (7) with the fitted K and H, with time expressed in days. The point at C_0 was treated as in Eq. (22). R^2 was calculated as in Eq. (16), with the observed and predicted rates in place of B. Neither model was re-estimated on the rates, so this comparison tests how well models fitted to concentration data reproduce the rates. The R^2 of Eq. (21) with the reported k ($\overline{r}_i = kC_i$, no intercept) was also calculated.

3.5 Linking degrader growth with the fitted kinetics

The degrader counts were not used in fitting, so they provide an internal check on the HM-FOKM. For each sampling interval i(from t_{i-1} to t_i, $\Delta t = 1$ week), the observed specific degradation rate was calculated from the TPH data as

$$k_{\mathrm{obs},i} = \frac{1}{\Delta t}\ln\left(\frac{C_{i-1}}{C_i}\right) \quad (27)$$

the degrader population over the interval as the geometric mean of the counts at its ends,

$$\bar{X}_i = \sqrt{X_{i-1}X_i} \quad (28)$$

and the specific activity per degrader as

$$a_i = \frac{k_{\mathrm{obs},i}}{\bar{X}_i} \quad (29)$$

Within each treatment (nine intervals), the Spearman rank correlation between k_{obs} and $\bar{X}$ tested whether the removal rate rose or fell as degraders grew, and the Pearson correlation between k_{obs} and the HM-FOKM rate $k(t) = K - Ht$ at the interval midpoint tested whether the fitted linear decline reproduced the observed rates. Between treatments ($n = 4$), H and K were correlated with the final degrader count and the time-averaged degrader count (trapezoidal mean over 0–9 weeks). With four treatments these between-treatment correlations are descriptive only.

4. Results

4.1 First-Order and HM-FOKM Fits

The HM-FOKM fitted the TPH data better than first-order kinetics in all four treatments (Tables 1 and 2, Figure 1). R^2 rose from 0.905–0.931 to 0.976–0.986, and RMSE fell by about half, from 0.032–0.063 to 0.014–0.030. The improvement outweighed the penalty for the extra parameter: ΔAICc was 9.8–12.8, which is strong (BA) to very strong (NA, BA+BS, BS) support for the HM-FOKM. The F-statistic was 21.5–31.6, well above the critical value of 5.32.

The first-order residuals were systematic. The model under-predicted removal for the first 4–7 weeks and over-predicted it for the last 2–5 weeks in every treatment, which is the pattern expected when the rate falls over time. The HM-FOKM residuals changed sign more often and showed no such trend (Supplementary Table S3 and Fig. S2).

Table 1. First-order and HM-FOKM parameter estimates (95% profile-likelihood intervals in brackets), with the first-order rate constants reported by Yaman (2020)

Treatment	First-order k(week^{-1})	HM-FOKM K(week^{-1})	HM-FOKM H(week^{-2})	Yaman (2020) k(week^{-1})
NA	0.060 [0.053, 0.067]	0.087 [0.075, 0.099]	0.0081 [0.0048, 0.0114]	0.111
BA+BS	0.192 [0.164, 0.225]	0.272 [0.230, 0.315]	0.0279 [0.0151, 0.0404]	0.293
BA	0.068 [0.060, 0.077]	0.099 [0.083, 0.115]	0.0093 [0.0047, 0.0138]	0.231
BS	0.155 [0.132, 0.183]	0.231 [0.196, 0.268]	0.0252 [0.0147, 0.0356]	0.233

Yaman (2020) $k$values are the reported 0.0159, 0.0419, 0.033 and 0.0333 d^{-1} multiplied by 7.

Table 2. Goodness of fit and model comparison ($n = 10$ per treatment)

Treatment	R^2FO	R^2HM	R^2Yaman k	RMSE FO	RMSE HM	RMSE Yaman k	AICc FO	AICc HM	ΔAICc	F
NA	0.931	0.986	−0.66	0.032	0.014	0.156	−66.6	−79.3	12.8	31.6
BA+BS	0.926	0.982	0.64	0.061	0.030	0.134	−53.5	−64.2	10.7	24.2
BA	0.911	0.976	−6.56	0.037	0.019	0.339	−63.6	−73.4	9.8	21.5
BS	0.905	0.980	0.57	0.063	0.029	0.133	−52.8	−65.0	12.2	29.4

$\Delta\text{AICc} = \text{AICc}(\text{first-order}) - \text{AICc}(\text{HM-FOKM})$; positive values favour the HM-FOKM. F is compared with $F_{0.05}(1, 8) = 5.32$. A negative R^2 means the prediction is worse than the mean of the data.

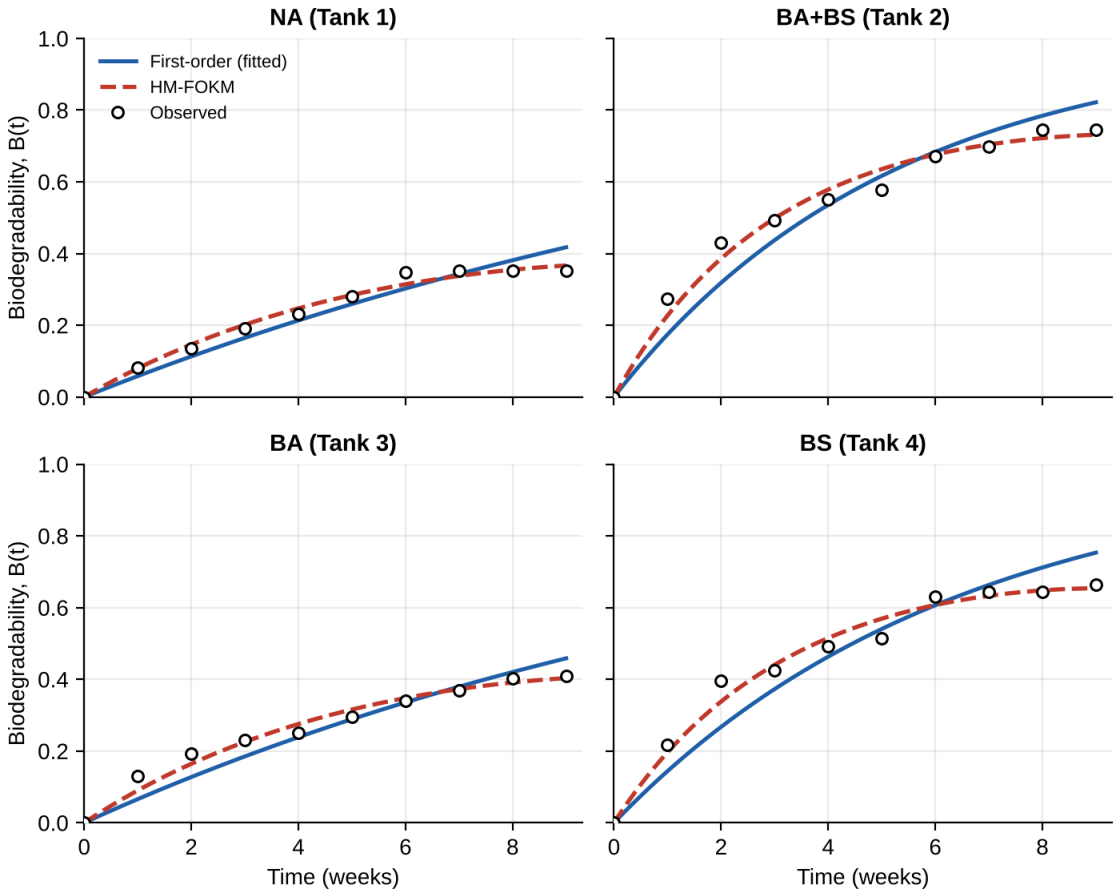


Figure 1. Observed TPH biodegradability (points) with the fitted first-order model (blue, solid), the HM-FOKM (red, dashed) and the first-order model using the rate constants reported by Yaman (2020) (grey, dotted).

4.2 Reconstruction of the Reported Rate Constants

The first-order rate constants reported by Yaman (2020) did not reproduce the measured TPH data (Table 2, Figure 1). They predicted day-63 biodegradability of 0.63–0.93 against observed values of 0.35–0.75, and gave negative R^2 for NA (−0.66) and BA (−6.56). They were 1.5–3.4 times larger than the first-order constants fitted directly to B(t). The largest discrepancy was for BA, whose reported constant (0.231 $week^{-1}$) was almost equal to that of BS (0.233 $week^{-1}$) although BA removed 41% of TPH and BS removed 66%.

To understand why the reported constants differ from the fitted ones, the procedure used to obtain them was reconstructed from the digitised data (Section 3.4). The procedure regresses the average removal rate since day 0 on concentration, with an intercept (Eqs. 22 and 23). Applying it to the digitised data reproduced the reported constants (Table 3): slopes of 0.0154, 0.0419, 0.0332 and 0.0340 d^{-1} against the reported 0.0159, 0.0419, 0.033 and 0.0333 d^{-1}, and R^2 values of 0.87, 0.89, 0.89 and 0.84 against the reported 0.86, 0.89, 0.88 and 0.84. The reported R^2 values are therefore correct for the calculation that produced them; the small differences reflect digitisation.

The intercepts were not negligible. They were −5.4 and −22.8 mg kg^{-1} d^{-1} for NA and BA, and +3.8 and +1.7 mg kg^{-1} d^{-1} for BA+BS and BS. When the intercept was removed, so that the reported k was tested as the first-order rate law it stands for (Eq. 21), R^2 fell to −2.38 for NA and −8.74 for BA, and to 0.84 and 0.81 for BA+BS and BS. For NA and BA, the high R^2 of the regression was carried by the intercept, not by the first-order term.

The procedure also did not recover the first-order constant from exact first-order data. Applied to the first-order curves fitted in this study, it returned slopes of 0.030, 0.109, 0.035 and 0.086 $week^{-1}$ for NA, BA+BS, BA and BS, only 0.51–0.57 of the first-order k that generated them (0.060, 0.192, 0.068 and 0.155 $week^{-1}$), together with positive intercepts of 7–19 mg kg^{-1} d^{-1}, as predicted by Eq. (24) and shown in Figure 2. The slopes obtained from the measured data (0.108, 0.293, 0.232 and 0.238 $week^{-1}$) were 2.7–6.7 times larger than these. The measured rate fell faster than the concentration, which steepened the rate–concentration line and offset the averaging bias. As a result, the reported constants came close to the HM-FOKM initial rate K in BA+BS (0.293 against 0.272 $week^{-1}$) and BS (0.233 against 0.231 $week^{-1}$), less so in NA (0.111 against 0.087 $week^{-1}$), and not in BA (0.231 against 0.099 $week^{-1}$). Applied to the fitted HM-FOKM curves, the procedure returned 0.111, 0.212, 0.117 and 0.198 $week^{-1}$.

Table 3. Rate constants of Yaman (2020) reproduced from the digitised data, and behaviour of the procedure on model curves

Quantity	NA	BA+BS	BA	BS
Regression of average rate on concentration (Eqs. 22, 23)				
Slope k, this study (d^{-1})	0.0154	0.0419	0.0332	0.0340
$k$reported by Yaman (2020) (d^{-1})	0.0159	0.0419	0.033	0.0333
Intercept a, this study (mg kg^{-1} d^{-1})	−5.4	3.8	−22.8	1.7
R^2, repeat of Yaman (2020), this study	0.87	0.89	0.89	0.84
R^2reported by Yaman (2020)	0.86	0.89	0.88	0.84
$R^2$of $r = kC$(Eq. 21), reported k	−2.38	0.84	−8.74	0.81
Slope from Eqs. (22) and (23) applied to ($week^{-1}$)				
Measured data	0.108	0.293	0.232	0.238
Exact first-order curve (Eq. 4, fitted k)	0.030	0.109	0.035	0.086
HM-FOKM curve (Eq. 7)	0.111	0.212	0.117	0.198
For reference: fitted first-order k	0.060	0.192	0.068	0.155
For reference: HM-FOKM K	0.087	0.272	0.099	0.231

Slopes in the second block are converted to $week^{-1}$ for comparison with $k$and K(Table 1). Ten points per treatment for the average rate (including the C_0point, assigned the first-week rate).

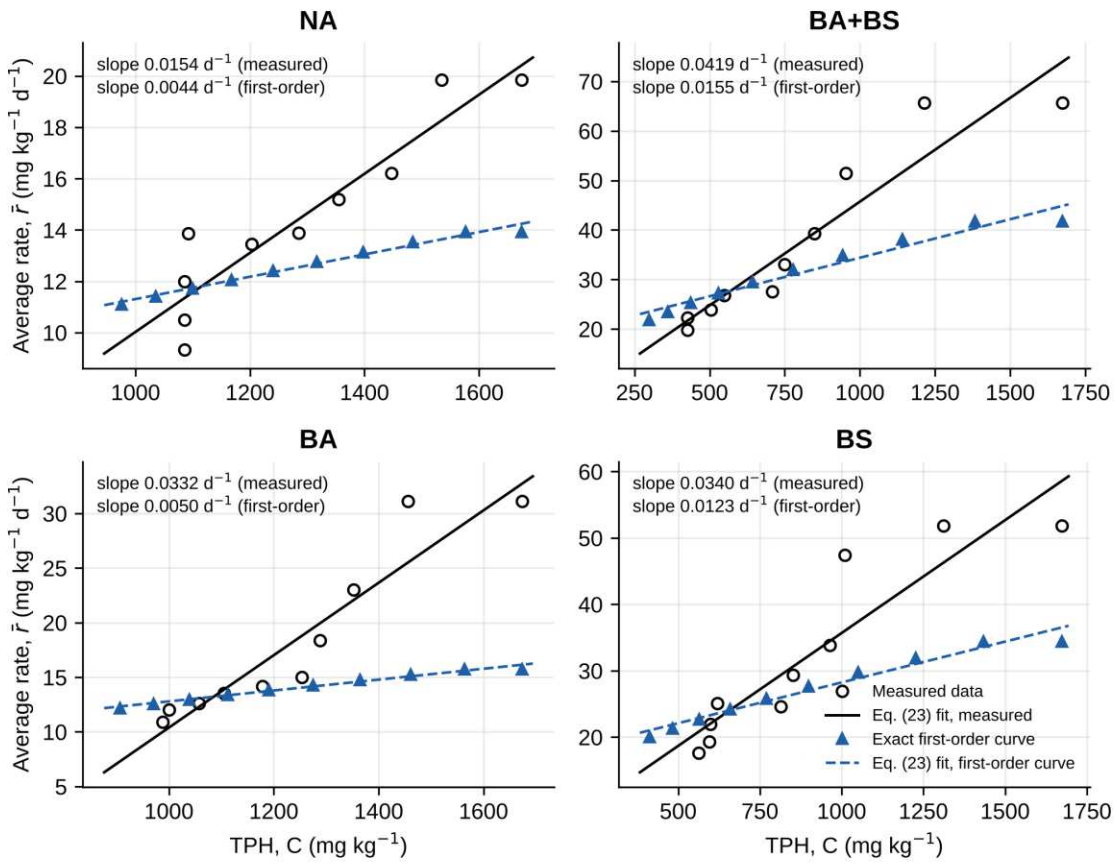


Figure 2. Average removal rate (Eq. 22) against TPH concentration for the measured data (circles) and for the exact first-order curve fitted in this study (triangles), each with the straight line of Eq. (23); slopes are in d^{-1}. The first-order constants that generated the triangles are 0.0086, 0.0274, 0.0097 and 0.0222 d^{-1} for NA, BA+BS, BA and BS, so the procedure recovers only 0.51–0.57 of the true constant. The slopes from the measured data are 2.7–6.7 times larger than those from the first-order curves.

4.3 Comparison of the Fitted Models in Rate Space

When the fitted models were compared in rate space (Eqs. 25 and 26), the HM-FOKM gave a higher R^2 than first-order kinetics for both the average and the weekly rate in all four treatments (Table 4). For the average rate, its R^2 was 0.94, 0.89, 0.62 and 0.93 for NA, BA+BS, BA and BS, compared with 0.18, 0.51, −0.04 and 0.45 for the fitted first-order model. For the weekly rate, the values were 0.67, 0.82, 0.64 and 0.70 for the HM-FOKM and 0.29, 0.64, 0.31 and 0.50 for the fitted first-order model. Although it was fitted to B(t) and not to the rates, the HM-FOKM matched or exceeded the regression R^2 of Yaman (2020) in NA, BA+BS and BS, and fell below it only in BA (0.62 against 0.89).

The first-order model described the rates poorly, with R^2 between −0.04 and 0.64, because a single constant cannot follow a rate that declines over time (Section 4.7). The HM-FOKM, which allows k to decline, described the concentrations, the average rate and the weekly rate.

Table 4. R^2 of the fitted first-order model and the HM-FOKM in rate space

Quantity	NA	BA+BS	BA	BS
R^2 for the average rate $\bar{r}$ (Eqs. 22, 26)				
First-order, fitted (Eq. 4)	0.18	0.51	−0.04	0.45
HM-FOKM (Eq. 7)	0.94	0.89	0.62	0.93
R^2 for the weekly rate r (Eqs. 25, 26)				
First-order, fitted (Eq. 4)	0.29	0.64	0.31	0.50
HM-FOKM (Eq. 7)	0.67	0.82	0.64	0.70

Ten points per treatment for the average rate (including the C_0 point, assigned the first-week rate) and nine for the weekly rate. The fitted first-order model and the HM-FOKM were fitted to $B(t)$ (Section 3.2) and were not re-estimated on the rates. A negative R^2 means the prediction is worse than the mean of the data.

4.4 Hindrance Coefficient, Transition Time, t_{50} and t_{90}

The hindrance coefficient was positive in all four treatments, and its 95% profile-likelihood interval excluded zero in every case (Table 1). Degradation therefore slowed significantly over the 63 days in all tanks, including the untreated control.

H increased in proportion to K. The ratio H/K was 0.093–0.109 week^{-1} across treatments, so the transition time t_trans = K/H fell in a narrow range of 9.2–10.8 weeks, just after the end of monitoring (Table 5). The projected biodegradability B_proj was within 0.024 of the observed week-9 value in every treatment. Because B_proj was below 0.9 in every treatment and below 0.5 for NA and BA, the HM-FOKM gives no t_{90} for any treatment and no t_{50} for NA or BA.

Table 5. Transition time, projected biodegradability and times to 50% and 90% removal from the HM-FOKM, with first-order values for comparison

Treatment	t_{trans} (weeks)	B_{proj}	Observed B at 9 weeks	t_{50} HM-FOKM (weeks)	t_{90} HM-FOKM (weeks)	t_{50} first-order (weeks)	t_{90} first-order (weeks)
NA	10.8	0.375	0.351	not reached	not reached	11.6	38.4
BA+BS	9.7	0.733	0.745	3.0	not reached	3.6	12.0
BA	10.7	0.411	0.410	not reached	not reached	10.2	33.8
BS	9.2	0.654	0.664	3.8	not reached	4.5	14.8

t_{trans} from Eq. (9); B_{proj} from Eq. (11); HM-FOKM t_{50} and t_{90} from Eq. (13); first-order values from Eq. (14). "Not reached": B_{proj} is below the target fraction, so Eq. (13) has no real solution. Monitoring period = 9 weeks (63 days).

The three approaches gave very different times to 50% and 90% removal (Tables 5 and 6). Only BA+BS and BS reached 50% removal during the experiment, at about 3.1 and 4.4 weeks (interpolated between sampling times). The HM-FOKM estimated 3.0 and 3.8 weeks, and the fitted first-order model 3.6 and 4.5 weeks. The half-lives reported by Yaman (2020) for these two tanks were shorter, 2.4 and 3.0 weeks, and across all four tanks the measured removal at the reported half-life was only 23–45%. For NA and BA, which never reached 50%, the reported half-lives (6.2 and 3.0 weeks) fall inside the monitoring period, the fitted first-order model places t_{50} just beyond it (11.6 and 10.2 weeks), and the HM-FOKM indicates that 50% would not be reached. For t_{90} the contrast is larger: the Yaman (2020) constants imply 7.9–20.7 weeks, the fitted first-order model 12.0–38.4 weeks, and the HM-FOKM no t_{90} at all.

Table 6. Observed time to 50% removal and the times implied by the kinetics reported by Yaman (2020)

Treatment	t_{50} observed (weeks)	Removal at 9 weeks	t_{50} reported by Yaman (2020) (weeks)	Removal observed at the reported t_{50}	t_{90} implied by Yaman (2020) k (weeks)
NA	not reached	35%	6.2	35%	20.7
BA+BS	3.1	75%	2.4	45%	7.9
BA	not reached	41%	3.0	23%	10.0
BS	4.4	66%	3.0	42%	9.9

Observed t_{50} was interpolated linearly between sampling times. The reported t_{50} is the half-life given by Yaman (2020) (43.6, 16.54, 21.0 and 20.8 d) divided by 7; removal at that time was interpolated from the digitised data. $t_{90} = \ln 10 / k$ using the reported constants.

4.5 Degrader Dynamics and TPH Removal

Degrader counts and TPH removal followed different time courses (Figure 3). Degrader numbers rose throughout the 63 days, from 1×10^5 CFU g^{-1} to 4.8×10^6 (NA), 40×10^6 (BA), 83×10^6 (BS) and 100×10^6 CFU g^{-1} (BA+BS). Growth was fastest between weeks 4 and 7, when BA+BS gained 58×10^6 CFU g^{-1} compared with 30×10^6 in weeks 0–4. TPH removal, in contrast, was fastest in the first week (460 mg kg^{-1} week^{-1} in BA+BS, 363 in BS, 218 in BA and 139 in NA) and averaged only 2–40 mg kg^{-1} week^{-1} over the last three weeks. The slowdown described by H therefore occurred while degrader populations were still growing.

The final degrader counts ranked the treatments in the same order as final TPH removal and as K: BA+BS > BS > BA > NA. All four tanks also showed a short rise in removal between days 35 and 42 (73–194 mg kg^{-1} week^{-1}), which in BA+BS, BA and BS coincided with the largest weekly increase in degrader numbers.

The yield coefficients reported by Yaman (2020) could be reproduced from the digitised data only after correcting their labels. The stated BA+BS value (80,300 CFU per mg TPH) was reproduced within 0.4%, but the values stated for BA (78,300) and BS (58,200) matched the data for BS (74,900) and BA (58,300), respectively, suggesting that the two labels were interchanged.

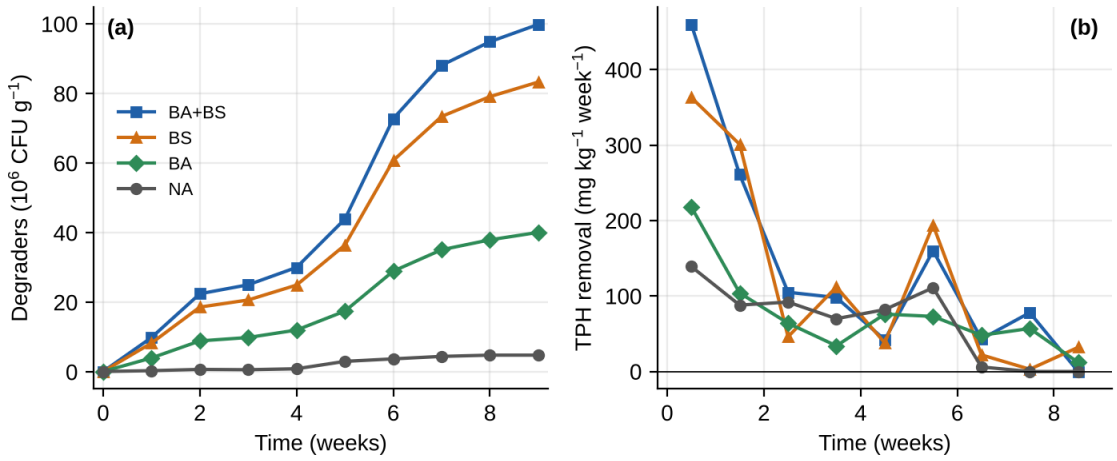


Figure 3. (a) Total hydrocarbon-degrading bacteria and (b) weekly TPH removal in each treatment, from the digitised data of Yaman (2020). Removal rates are plotted at the midpoint of each sampling interval.

4.6 Amendment Effects on K, H, t_{trans} and B_{proj}

The four tanks form a 2×2 design: inoculum (with or without) crossed with nutrients (with or without). Table 7 gives the effect of each amendment in the presence and absence of the other.

Nutrient addition had the largest effect on every parameter. It raised K by a factor of 2.7 and H by a factor of 3.0–3.1, whether or not the inoculum was present, and increased B_{proj} by 0.28–0.32 and observed removal at 9 weeks by 0.31–0.34. The 95% intervals for K did not overlap between nutrient-amended and unamended tanks. Nutrients also shortened t_{trans} by 1.0–1.6 weeks.

The inoculum had a much smaller effect. It raised K by 14–17% and B_{proj} by 0.04–0.08, and the intervals for K overlapped in both comparisons. Without nutrients, the inoculum increased the final degrader count 8.4-fold but K by only 14%.

The two amendments acted almost independently. The nutrient effect on K was the same with and without inoculum ($\times$ 2.74 vs $\times$ 2.66; ratio 1.03), and the inoculum added 0.08 to observed removal with nutrients and 0.06 without (difference 0.02).

Table 7. Effect of each amendment on the HM-FOKM parameters, observed removal and degrader counts

Comparison	Both tanks mixed daily	K ratio	H ratio	Δt_{trans} (weeks)	ΔB_{proj}	ΔB at 9 weeks	Degrader ratio at 9 weeks
Nutrients, without inoculum (BS vs NA)	No	2.66	3.12	−1.6	+0.28	+0.31	17.4
Nutrients, with inoculum (BA+BS vs BA)	Yes	2.74	3.02	−1.0	+0.32	+0.34	2.5

Inoculum, without nutrients (BA vs NA)	No	1.14	1.14	−0.1	+0.04	+0.06	8.4
Inoculum, with nutrients (BA+BS vs BS)	Yes	1.17	1.11	+0.6	+0.08	+0.08	1.2

Ratios and differences are amended minus (or divided by) unamended. Tank 1 (NA) was not mixed, so comparisons with NA also include the effect of daily mixing; the two comparisons between mixed tanks are free of this confounding.

4.7 Degrader Growth and the Hindrance Coefficient

Within every treatment, the observed specific degradation rate fell while the degrader population rose (Table 8, Figure 4). The Spearman correlation between k_{obs} and degrader count was negative in all four tanks ($\rho = -0.50$ to -0.63). Individually these correlations were not significant ($p = 0.07$–0.17, nine intervals each), but the sign was the same in every treatment. Mean k_{obs} fell from 0.070–0.227 week^{-1} in weeks 1–3 to 0.002–0.083 week^{-1} in weeks 7–9, while the mean degrader count over the same intervals increased 7–10-fold. The specific activity per degrader therefore fell by a factor of 74–510.

The HM-FOKM rate $k(t) = K - Ht$ reproduced the observed interval rates. The Pearson correlation between k_{obs} and $k(t)$ was 0.59–0.74 within treatments ($p = 0.02$–0.10) and 0.73 for the four treatments pooled ($n = 36$, $p < 0.001$). The constant first-order rate, by definition, cannot follow this decline (Figure 3).

Between treatments, H increased with degrader abundance. H was strongly correlated with the final degrader count (Pearson $r = 0.955$, $p = 0.045$; Spearman $\rho = 1.0$, exact $p = 0.083$) and with the time-averaged count ($r = 0.955$). K showed the same association ($r = 0.958$), and H and K were themselves almost perfectly correlated ($r = 0.997$). Treatments with larger degrader populations therefore started faster and slowed down more.

Table 8. Observed specific degradation rates, degrader counts and their correlations within each treatment (nine weekly intervals)

Treatment	Mean k_{obs}, weeks 1–3 (week^{-1})	Mean k_{obs}, weeks 7–9 (week^{-1})	Degraders at 9 weeks (10^6 CFU g^{-1})	Spearman ρ, k_{obs} vs $\bar{X}(p)$	Pearson r, k_{obs} vs $k(t)(p)$	Fall in specific activity a, weeks 1–3 to 7–9
NA	0.070	0.002	4.8	−0.63 (0.070)	0.74 (0.024)	510-fold
BA+BS	0.227	0.083	99.9	−0.57 (0.112)	0.63 (0.068)	121-fold
BA	0.087	0.037	40.1	−0.63 (0.067)	0.68 (0.043)	74-fold

BS	0.184	0.032	83.3	−0.50 (0.171)	0.59 (0.096)	227-fold

k_{obs} from Eq. (27), $\bar{X}$ from Eq. (28), a from Eq. (29); $k(t) = K - Ht$ evaluated at the interval midpoint. Pooled Pearson r between k_{obs} and $k(t)$ = 0.73 ($n = 36$, $p < 0.001$).

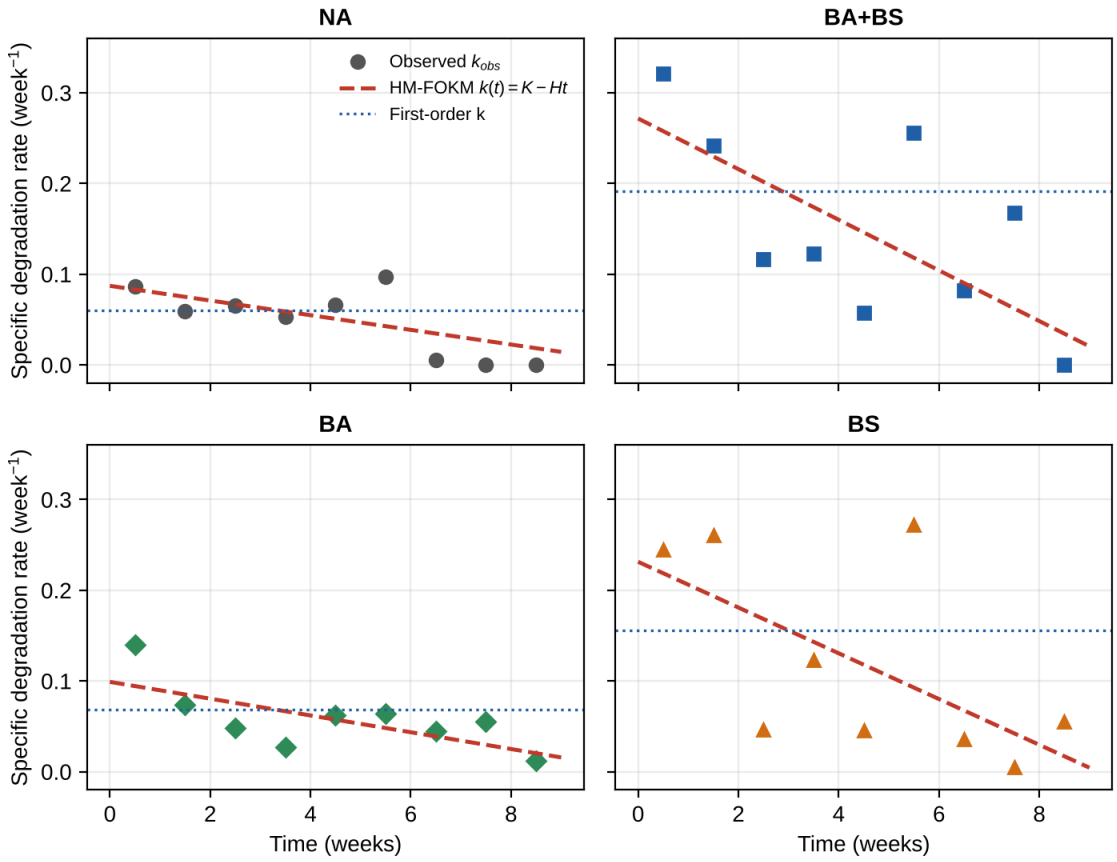


Figure 4. Observed specific degradation rate in each weekly interval (points, Eq. 27) with the HM-FOKM rate $k(t) = K - Ht$ (red, dashed) and the constant fitted first-order rate (blue, dotted). Degrader counts for the same tanks are shown in Figure 2a.

5.1 First-Order Kinetics versus the HM-FOKM

First-order kinetics assumes that the same fraction of the remaining TPH is removed each week. The Yaman (2020) data do not behave this way. In every tank the weekly fraction removed was largest at the start and smallest at the end, so a single rate constant had to compromise between the two phases. It was too low for the early weeks and too high for the late weeks, which produced the systematic residual pattern in Section 4.1 (Supplementary Fig. S2). This fast-then-slow behaviour is common in hydrocarbon-contaminated soil and is usually attributed to the exhaustion of the readily degradable fraction, declining bioavailability as the residue weathers and sorbs, and the build-up of inhibitory metabolites (Scow et al., 1986; Alexander, 1999; Smith et al., 1999; Ros et al., 2010; Jiang et al., 2016; Ramadass et al., 2018). Second-order kinetics has likewise fitted TPH removal better than first-order kinetics in other amended soils (Sarkar et al., 2005; Nwankwegu et al., 2016; Ritoré et al., 2026).

The HM-FOKM represents this behaviour with one additional parameter. Allowing the rate constant to decline linearly with time removed the residual trend, halved the RMSE and raised R^2 to 0.976–0.986 (Section 4.1, Table 2, Figure 1). The improvement was not an artefact of the extra parameter: AICc, which penalises the added parameter for the small sample, still favoured the HM-FOKM by 9.8–12.8 units, the F-test was significant at far beyond the 5% level, and the profile-likelihood interval for H excluded zero in every treatment (Table 1). With ten sampling times per treatment, the Yaman (2020) data contain enough information to establish the deceleration, not merely to accommodate it.

The HM-FOKM is therefore the better description of TPH removal in all four treatments. Its advantage is not only statistical. Its two parameters separate how fast degradation starts (K) from how quickly it slows (H), whereas a single first-order constant mixes the two. That distinction changes the conclusions drawn about the treatments and about how much further removal can be expected (Sections 5.3–5.5).

5.2 Re-evaluation of the Kinetic Results of Yaman (2020)

The reanalysis supports the main experimental conclusion of Yaman (2020): combined bioaugmentation and biostimulation removed the most TPH, followed by biostimulation, bioaugmentation and natural attenuation. It does not support the kinetic analysis, which contains several errors.

5.2.1 Rate Constants and Half-Lives

The first-order constants in Table 3 of Yaman (2020) were derived from plots of reaction rate against concentration (Figure 5 of that paper) rather than from the concentration–time data. They are 1.5–3.4 times larger than the constants fitted to the TPH series (Table 1) and predict day-63 removal of 63–93%, against measured values of 35–74% (Section 4.2, Table 2, Figure 1). The reported half-lives are inconsistent with the data in the same paper. A half-life of 43.6 days is reported for NA and 21.0 days for BA, yet neither tank reached 50% removal within the 63-day experiment (35% and 41%). For BA+BS, the reported half-life of 16.5 days compares with an observed time to 50% removal of 21–28 days, and for BS, 20.8 days compares with 28–35 days (Section 4.4, Table 6). The reported constant for BA (0.033 d^{-1}) is also almost the same as that for BS (0.0333 d^{-1}), although BS removed 25 percentage points more TPH.

5.2.2 The Rate–Concentration Procedure

The method used to obtain these constants has three weaknesses. First, the line fitted to the rate data had an intercept that was not reported, so the published R^2 values describe a two-parameter regression rather than the first-order rate law $r = kC$; without the intercept, the fit for NA and BA was worse than the mean of the data (Table 3). Second, the rates were averages since the start of treatment, not instantaneous rates. For first-order data the average rate is proportional to the logarithmic mean of C_0 and C rather than to C (Eq. 24), so the procedure returns only about half of the true constant (0.51–0.57 of k here) even when the first-order model is correct (Table 3, Figure 2). Third, the constants were converted to half-lives that assume a constant rate over the whole experiment, which the data do not support (Section 4.4, Table 6).

The closeness of the reported constants to the HM-FOKM K in BA+BS and BS is therefore not a validation of the procedure. It results from two opposing effects: the averaging bias, which lowers the slope, and the decline in the specific rate, which raises it. The second effect is itself evidence of hindrance. Had degradation been first-order, the procedure would have returned slopes 2.7–6.7 times smaller than it did (Table 3, Figure 2), and the negative intercepts for NA and BA indicate a rate that approaches zero while TPH remains, which is the slowdown the HM-FOKM describes with H. The reported constants are best read as rough indicators of the initial rate, not as time-

invariant first-order coefficients, and should not be used for half-lives or remediation forecasts. These criticisms concern the kinetic analysis only; the experimental design, the measured data and the ranking of the treatments in Yaman (2020) are unaffected.

5.2.3 The Monod Comparison

Yaman (2020) concluded that the Monod model fitted better than first-order kinetics, based on R^2 values of 0.89–0.97 for the rate data. Those R^2 values refer to the derived rates, not to the measured TPH concentrations, so they do not show that either model reproduces the concentration time series (Section 4.3, Table 4). The degrader data also argue against a Monod-type rate law in which the rate is proportional to biomass. Between week 1 and week 9, degrader numbers increased by a factor of 10 in BA+BS and BS, while weekly TPH removal fell by about 90–95% (from 460 to an average of 40 mg kg^{-1} $week^{-1}$ over the last three weeks in BA+BS, and from 363 to 19 in BS; Section 4.5, Figure 3). Because the rate in Monod-type models is proportional to biomass (Bekins et al., 1998; Ostendorf et al., 2007), a rate law driven by the measured degrader population would predict the opposite trend.

5.2.4 Microbial Results

Two statements about the microbial data are not supported by the digitised figures. The yield coefficients stated for BA and BS match the data only if their labels are interchanged (Section 4.5). The abstract also states that degrader numbers in tank 2 were two orders of magnitude higher than in the control. In the digitised data the ratio was 15–41 times (about 1.2–1.6 orders of magnitude) at the sampling times after day 0, and 21 times at day 63.

These inconsistencies do not affect the measured TPH and degrader time series, which agree with the values stated in the text. They affect the kinetic parameters derived from those data, which are the values most likely to be reused in remediation design.

5.3 Physical Interpretation of the Hindrance Coefficient

In the HM-FOKM, $H = \alpha(p - v)$, so a positive H indicates that whatever slows degradation accumulates faster than it is removed. H was positive in all four tanks, including tank 1, which was not mixed, and tanks 2–4, which were mixed daily (Table 1). Daily mixing for aeration was therefore not sufficient to prevent the slowdown.

The degrader data narrow the possible causes. Degradation slowed while degrader numbers were still rising (Section 4.5, Figure 3), so the slowdown was not caused by a shortage of degrading bacteria. It is more consistent with a limitation on the substrate side: depletion of the readily degradable fraction of the crude oil, declining bioavailability of the residue, or accumulation of inhibitory metabolites (Alexander, 1999; Smith et al., 1999; Jiang et al., 2016; Ramadass et al., 2018). The data cannot distinguish between these, because the four mechanistic quantities in K and H are lumped together (Section 2.2).

The proportionality between H and K points in the same direction. The ratio H/K, and hence t_trans, was nearly the same in all four tanks (9.2–10.8 weeks), although K differed by a factor of 3 (Table 5). The amendments increased the initial rate but did not extend the period over which degradation continued. A shared transition time is what would be expected if all four tanks were working on the same pool of degradable hydrocarbons in the same soil, with the amendments mainly changing how quickly that pool was consumed.

Internal validation from the degrader data. The degrader counts were not used to fit the HM-FOKM, so they offer an independent test of what H represents (Section 4.7). Three results agree. First, the observed specific rate fell in every tank while the degrader population grew 7–10-fold, and the activity per degrader fell 74–510-fold; the slowdown captured by H cannot therefore be a loss of degraders (Table 8). Second, the linear decline $k(t) = K -$

Ht reproduced the observed interval rates (pooled r = 0.73, p < 0.001; Table 8, Figure 4), which supports the central assumption of the model that the rate falls steadily with time. Third, between treatments H rose with degrader abundance. Because H was almost perfectly correlated with K (r = 0.997), this does not mean that bacteria cause hindrance; it means that the treatments that supported more degraders consumed the accessible hydrocarbons faster and so reached their limit sooner. This is consistent with the substrate-side interpretation above and with the similar t_trans in all tanks. The between-treatment correlations rest on four treatments and should be read as supporting, not conclusive, evidence; replicate degrader and TPH data from more treatments would allow a formal test.

5.4 Transition Time, t_{50} and t_{90}

Transition time. The transition time t_trans is the point at which the fitted degradation rate falls to zero, that is, the end of active degradation under the conditions present during the experiment. It was 9.2–10.8 weeks, or 1.02–1.20 times the 9-week monitoring period (Table 5). The experiment therefore covered almost the whole decelerating phase, which is why H could be estimated precisely, but it stopped just before the projected plateau. Monitoring to about 1.5 × t_trans, roughly 14–16 weeks here, would have been needed to confirm whether removal levels off or continues slowly. Because t_trans was nearly the same in all four tanks, a single sampling schedule would have served every treatment.

Time to 50% removal. For a decelerating trajectory the first-order half-life is not a constant: under the HM-FOKM each successive halving takes longer than the last, so t_{50} is better reported as the time to reach a removal target than as a half-life. Measured against the data, the HM-FOKM reproduced the observed t_{50} of BA+BS (3.0 vs 3.1 weeks), whereas the fitted first-order model was 0.5 weeks late (Tables 5 and 6). For BS the HM-FOKM was 0.6 weeks early and first-order matched the observed value (4.5 vs 4.4 weeks), because the week-5 measurement fell below both fitted curves (Figure 1). The half-lives reported by Yaman (2020) were 24–33% shorter than the observed t_{50} for BA+BS and BS (Section 5.2.1). For NA and BA they placed 50% removal at 6.2 and 3.0 weeks, inside the experiment, although neither tank reached 50% removal at any time (Table 6).

Projected biodegradability. Where t_{50} or t_{90} does not exist, B_{proj} is the more informative measure. It is the maximum fraction of TPH the HM-FOKM expects to be removed under the conditions of the experiment, reached at t_{trans}. For NA and BA, B_{proj} was 0.375 and 0.411, so the fitted rate falls to zero before half of the TPH has gone and Eq. (13) has no real solution for $x = 0.5$. For all four treatments B_{proj} was below 0.9, so no t_{90} exists. B_{proj} also shows how far each tank already was from its limit: the observed removal at week 9 was within 0.024 of B_{proj} in every treatment (Table 5), so each tank had already achieved almost all the removal it could achieve under its initial conditions.

Table 8. Residual TPH at the projected plateau

Treatment	Residual TPH at plateau, $C_0(1 - B_{\mathrm{proj}})$ (mg kg^{-1})	Removal still needed for 90% (mg kg^{-1})
BA+BS	447	280
BS	579	412
BA	986	819
NA	1046	879

$C_0 = 1674$mg kg^{-1}; 90% removal corresponds to 167 mg kg^{-1}.

Expressed as concentrations (Table 8), the plateau leaves 447–1046 mg kg^{-1} of TPH in the soil, 280–879 mg kg^{-1} more than a 90% target would allow. This gap, rather than a time, is the quantity a remediation plan needs: it shows that even the best treatment would stop about 17 percentage points short of 90% removal without a further intervention, and that NA and BA would achieve less than half of the removal a 90% target requires. First-order kinetics hides this gap because it assumes removal continues indefinitely, which is why it predicts finite $t_{50}$and t_{90}values for every treatment.

Time to 90% removal. The largest practical difference is in t_{90}. With the constants reported by Yaman (2020), BA+BS would have reached 90% removal at 7.9 weeks, before the end of the experiment, yet the measured removal at 9 weeks was 74.5% (Table 6). The fitted first-order model moves $t_{90}$to 12.0–38.4 weeks, and the HM-FOKM indicates that 90% removal is not reachable under the conditions of the experiment, with removal levelling off at 38–73% (B_{proj}; Table 5). A remediation plan built on first-order kinetics would therefore either end treatment too early or promise an outcome the data do not support. The HM-FOKM instead signals that a further intervention, such as renewed nutrient addition, re-inoculation or measures that restore bioavailability, would be needed before t_{trans}if a 90% target is required.

Caveat on the plateau. Holding Bconstant after $t_{\mathrm{trans}}$is a modelling choice (Section 2.3). The last observed values for BA+BS and BS were slightly above B_{proj}(by 0.012 and 0.010), which suggests slow residual removal that the plateau does not capture. "Not reached" should therefore be read as not reached at the rate described by the first 9 weeks; the true t_{90}may be finite but much longer than first-order kinetics predicts.

5.5 Amendment Effects: A Rate–Curvature–Persistence Perspective

5.5.1 From Endpoint Removal to Temporal Behaviour

Yaman (2020) compared the treatments mainly through TPH removal at day 63 and first-order rate constants. Both compress the trajectory into one number. The HM-FOKM separates four aspects of performance: how fast degradation starts (K), how quickly it slows (H), how long it persists (t_{trans}) and how far it can go (B_{proj}). Comparing the treatments on all four shows what each amendment changed.

5.5.2 The Ranking

Table 9 ranks the treatments on each descriptor. The ranks for K, H, B_{proj}, observed removal and final degrader count were identical: BA+BS > BS > BA > NA. Persistence ranked in nearly the opposite order: the two nutrient-amended tanks, which started fastest, reached t_{trans}1–1.6 weeks earlier (9.2–9.7 weeks) than NA and BA (10.7–10.8 weeks), and their H/Kratio was slightly higher (0.103–0.109 vs 0.093 week^{-1}). Faster degradation was therefore bought with a slightly shorter active period.

Table 9. Rate–curvature–persistence ranking of the treatments (rank in brackets)

Treatment	K(week^{-1})	H(week^{-2})	t_{trans}(weeks)	B_{proj}	Observed B at 9 weeks	Degraders at 9 weeks (10^6 CFU g^{-1})
BA+BS	0.272 (1)	0.0279 (1)	9.7 (3)	0.733 (1)	0.745 (1)	99.9 (1)
BS	0.231 (2)	0.0252 (2)	9.2 (4)	0.654 (2)	0.664 (2)	83.3 (2)
BA	0.099 (3)	0.0093 (3)	10.7 (2)	0.411 (3)	0.410 (3)	40.1 (3)
NA	0.087 (4)	0.0081 (4)	10.8 (1)	0.375 (4)	0.351 (4)	4.8 (4)

Rank 1 denotes the highest K, H, B_{proj}, removal and degrader count, and the longest t_{trans}.

5.5.3 Why Initial Rate Predicted Endpoint Performance Here

The treatment that degrades fastest at first is not always the one that removes the most by the end. Here it was, and the HM-FOKM explains why. Because $K^2/2H = K \cdot t_{\text{trans}}/2$, Eq. (11) can be written as $B_{\text{proj}} = 1 - \exp(-K \cdot t_{\text{trans}}/2)$. When t_{trans} is similar across treatments, as it was here (9.2–10.8 weeks; Table 9), B_{proj} is set mainly by K, so the treatment that starts fastest also removes the most. Where amendments change t_{trans} substantially, the two rankings can diverge, and K alone would be a misleading guide.

5.5.4 Nutrients versus Inoculum

Nutrient addition was the dominant amendment. It roughly tripled K and H and added about 0.3 to B_{proj}, and it did so with or without the inoculum (Table 7). This is consistent with the strong nutrient deficiency of the original soil, whose nitrogen and phosphorus contents were far below those needed for the C:N:P ratio of 100:5:1 targeted by Yaman (2020), and with earlier reports of nutrient-limited crude-oil degradation (Chaîneau et al., 2005). The inoculum alone raised the final degrader count 8.4-fold but K by only 14%, so most of the added cells contributed little activity while nutrients were limiting, a pattern also reported where biostimulation outperformed bioaugmentation (Kauppi et al., 2011; Nikolopoulou et al., 2013; Abed et al., 2014). With nutrients present, the inoculum added a modest 17% to K and 0.08 to B_{proj}. The near-zero interaction (Section 4.6) indicates that the two amendments acted independently rather than synergistically.

The design has one confounding factor. Tank 1 (NA) was not mixed, whereas tanks 2–4 were mixed daily for aeration. The two comparisons between mixed tanks (BA+BS vs BA, and BA+BS vs BS) are free of this confounding, and they gave nearly the same effects as the comparisons with NA (Table 7). The combined effect of mixing and inoculum in BA relative to NA was also small ($K \times 1.14$). Daily mixing therefore appears to have had little effect on K in this soil, although the design cannot separate it formally.

5.5.5 Implications

For this soil, nutrients are the main lever and bioaugmentation adds a modest benefit only when nutrients are supplied. Neither amendment extended the period of active degradation; nutrients shortened it slightly. Raising removal beyond B_{proj}would therefore require a further intervention around t_{trans}, such as a second nutrient dose, rather than a larger single dose at the start or a longer treatment period. These conclusions rest on treatment means without published dispersion and on a single soil, and should be tested with replicated designs that include a mixed, unamended control.

5.6 Practical Implications

The two models lead to different remediation forecasts (Section 5.4). First-order kinetics implies continued removal towards 90%, whereas the HM-FOKM indicates that removal levels off close to the values already reached at week 9 (75% for BA+BS, 66% for BS, 41% for BA and 35% for NA). A plan based on first-order kinetics would therefore overestimate the removal achievable with these treatments and underestimate the time and further intervention needed to reach a regulatory target.

The amendment comparison (Section 5.5) identifies nutrient supply as the main lever in this soil, with bioaugmentation adding a modest benefit only when nutrients are supplied. Because no amendment extended the transition time, extending the treatment period beyond about 10 weeks is unlikely to bring much further removal without a second intervention, such as renewed nutrient addition or a change in conditions that restores bioavailability.

More generally, kinetic parameters for soil remediation should be estimated by fitting the integrated rate law directly to the concentration data, and the fitted model should be checked against the measured series before half-lives or remediation times are reported (Adair et al., 2010; Escuder-Gilabert et al., 2019).

6. Conclusions

This study developed the hindrance-modified first-order kinetic model (HM-FOKM), applied it to the pilot-scale data of Yaman (2020) for crude-oil-contaminated soil, and compared it with first-order kinetics. The main conclusions are:

1. **TPH removal slowed significantly over the 63 days in all four treatments.** First-order kinetics could not represent this: it under-predicted early removal and over-predicted late removal in every tank (Section 4.1, Figure 1). The residuals of the first-order model were systematic in every treatment, whereas the HM-FOKM residuals showed no such trend (Supplementary Fig. S2).

2. **The HM-FOKM was the better model in all four treatments.** It raised R^2 from 0.905–0.931 to 0.976–0.986, halved the RMSE, and was favoured by AICc by 9.8–12.8 units (Section 4.1, Table 2). The hindrance coefficient H was positive, and its 95% profile-likelihood interval excluded zero in every treatment (Table 1).

3. **The first-order rate constants and half-lives reported by Yaman (2020) are not consistent with the measured data.** They were obtained by regressing the average rate since day 0 on concentration with an unreported intercept, a procedure that returns only about half of the true constant even for first-order data (Section 4.2, Table 3, Figure 2). The reported rate constants were 1.5–3.4 times larger than the fitted first-order constants, and the reported half-lives for natural attenuation and bioaugmentation were shorter than the 63-day experiment although neither treatment reached 50% removal (Section 4.4, Table 6). The

reported yield coefficients for bioaugmentation and biostimulation also appear to have been interchanged (Section 4.5).

4. **Degradation slowed while the degrader population was still growing, in all four tanks.** The slowdown is therefore more consistent with substrate-side limitation, such as depletion of the readily degradable fraction or declining bioavailability, than with a shortage of degrading bacteria (Section 4.5, Figure 3). The observed specific rate fell 74–510-fold per degrader over the experiment (Table 8), and the measured biomass does not support a Monod-type rate law in which the rate is proportional to biomass (Section 5.2.3).

5. **Nutrient addition was the main driver of performance, raising the initial rate K by a factor of 2.7.** Bioaugmentation alone had little effect (Section 4.6, Table 7). Because H rose in proportion to K, all treatments reached the transition time at about 9–11 weeks, and the HM-FOKM projects that removal would level off at about 38–73% rather than continue to 90% as first-order kinetics implies (Section 4.4, Table 5).

Kinetic parameters for soil remediation should be estimated by fitting the integrated rate law directly to concentration–time data and checked against the measurements before half-lives or remediation times are reported. Where the removal rate declines over time, the HM-FOKM provides a simple, nested alternative to first-order kinetics that gives more realistic forecasts of achievable removal. Longer monitoring and fractionated hydrocarbon analysis are needed to confirm the projected plateau and to identify the cause of the slowdown.

References

Abed RMM, Al-Sabahi J, Al-Maqrashi F, Al-Habsi A, Al-Hinai M (2014) Characterization of hydrocarbon-degrading bacteria isolated from oil-contaminated sediments in the Sultanate of Oman and evaluation of bioaugmentation and biostimulation approaches in microcosm experiments. Int Biodeterior Biodegrad 89:58–66

Adair EC, Hobbie SE, Hobbie RK (2010) Single-pool exponential decomposition models: potential pitfalls in their use in ecological studies. Ecology 91:1225–1236

Agamuthu P, Tan YS, Fauziah SH (2013) Bioremediation of hydrocarbon contaminated soil using selected organic wastes. Procedia Environ Sci 18:694–702

Alao JO, Saqr AM, Ayejoto DA, Otorkpa OJ, Abubakar F, Mohammed MAA, Ibe AA (2025) Environmental impacts of hydrocarbon contaminants and associated potential public health risks. J Hazard Mater Adv 19:100853

Alexander M (1999) Biodegradation and bioremediation, 2nd edn. Academic Press, San Diego

Bates DM, Watts DG (1988) Nonlinear regression analysis and its applications. Wiley, New York

Bekins BA, Warren E, Godsy EM (1998) A comparison of zero-order, first-order, and Monod biotransformation models. Ground Water 36:261–268

Burnham KP, Anderson DR (2002) Model selection and multimodel inference: a practical information-theoretic approach, 2nd edn. Springer, New York

Cerqueira VS, Peralba MCR, Camargo FAO, Bento FM (2014) Comparison of bioremediation strategies for soil impacted with petrochemical oily sludge. Int Biodeterior Biodegrad 95:338–345

Chaîneau CH, Rougeux G, Yéprémian C, Oudot J (2005) Effects of nutrient concentration on the biodegradation of crude oil and associated microbial populations in the soil. Soil Biol Biochem 37:1490–1497

Drevon D, Fursa SR, Malcolm AL (2017) Intercoder reliability and validity of WebPlotDigitizer in extracting graphed data. Behav Modif 41:323–339

Escuder-Gilabert L, Martín-Biosca Y, Sagrado S, Medina-Hernández MJ (2019) Anticipating the impact of pitfalls in kinetic biodegradation parameter estimation from substrate depletion curves of organic pollutants. Environ Pollut 252:128–136

Hurvich CM, Tsai C-L (1989) Regression and time series model selection in small samples. Biometrika 76:297–307

Jiang Y, Brassington KJ, Prpich G, Paton GI, Semple KT, Pollard SJT, Coulon F (2016) Insights into the biodegradation of weathered hydrocarbons in contaminated soils by bioaugmentation and nutrient stimulation. Chemosphere 161:300–307

Kauppi S, Sinkkonen A, Romantschuk M (2011) Enhancing bioremediation of diesel-fuel-contaminated soil in a boreal climate: comparison of biostimulation and bioaugmentation. Int Biodeterior Biodegrad 65:359–368

Komilis DP, Vrohidou A-EK, Voudrias EA (2010) Kinetics of aerobic bioremediation of a diesel-contaminated sandy soil: effect of nitrogen addition. Water Air Soil Pollut 208:193–208

Koshlaf E, Ball AS (2017) Soil bioremediation approaches for petroleum hydrocarbon polluted environments. AIMS Microbiol 3:25–49

Leahy JG, Colwell RR (1990) Microbial degradation of hydrocarbons in the environment. Microbiol Rev 54:305–315

Lee H, Sam K, Coulon F, De Gisi S, Notarnicola M, Labianca C (2024) Recent developments and prospects of sustainable remediation treatments for major contaminants in soil: a review. Sci Total Environ 912:168769

Liu Q, Li Q, Wang N, Liu D, Zan L, Chang L, Gou X, Wang P (2018) Bioremediation of petroleum-contaminated soil using aged refuse from landfills. Waste Manag 77:576–585

Mancera-López ME, Esparza-García F, Chávez-Gómez B, Rodríguez-Vázquez R, Saucedo-Castañeda G, Barrera-Cortés J (2008) Bioremediation of an aged hydrocarbon-contaminated soil by a combined system of biostimulation–bioaugmentation with filamentous fungi. Int Biodeterior Biodegrad 61:151–160

Margesin R, Schinner F (2001) Bioremediation (natural attenuation and biostimulation) of diesel-oil-contaminated soil in an alpine glacier skiing area. Appl Environ Microbiol 67:3127–3133

Mekonnen BA, Aragaw TA, Genet MB (2024) Bioremediation of petroleum hydrocarbon contaminated soil: a review on principles, degradation mechanisms, and advancements. Front Environ Sci 12:1354422

Mohanta S, Pradhan B, Behera ID (2024) Impact and remediation of petroleum hydrocarbon pollutants on agricultural land: a review. Geomicrobiol J 41:345–359

Momoh Y (2025) Modifying the Baranyi-Roberts model for studying bio-remediation kinetics in crude-oil contaminated soil. Discov Soil 2:52. https://doi.org/10.1007/s44378-025-00071-2

Nikolopoulou M, Pasadakis N, Kalogerakis N (2013) Evaluation of autochthonous bioaugmentation and biostimulation during microcosm-simulated oil spills. Mar Pollut Bull 72:165–173

Nwankwegu AS, Orji MU, Onwosi CO (2016) Studies on organic and in-organic biostimulants in bioremediation of diesel-contaminated arable soil. Chemosphere 162:148–156

Odermatt JR (1997) Simulations of intrinsic biodegradation using a nonlinear modification of first-order reaction kinetics. J Soil Contam 6:495–508

Ostendorf DW, Hinlein ES, Schoenberg TH, DeFlaun MF (2007) Monod kinetics for aerobic biodegradation of petroleum hydrocarbons in unsaturated soil microcosms. Environ Sci Technol 41:2347–2353

Polyak YM, Bakina LG, Chugunova MV, Mayachkina NV, Gerasimov AO, Bure VM (2018) Effect of remediation strategies on biological activity of oil-contaminated soil – a field study. Int Biodeterior Biodegrad 126:57–68

Ramadass K, Megharaj M, Venkateswarlu K, Naidu R (2018) Bioavailability of weathered hydrocarbons in engine oil-contaminated soil: impact of bioaugmentation mediated by *Pseudomonas* spp. on bioremediation. Sci Total Environ 636:968–974

Raue A, Kreutz C, Maiwald T, Bachmann J, Schilling M, Klingmüller U, Timmer J (2009) Structural and practical identifiability analysis of partially observed dynamical models by exploiting the profile likelihood. Bioinformatics 25:1923–1929

Ritoré E, Arnaiz C, Morillo J, Egea-Corbacho A, Usero J (2025) Use of liquid industrial by-products as biostimulants in the remediation of hydrocarbon-contaminated soils. Clean Technol 7:114. https://doi.org/10.3390/cleantechnol7040114

Ritoré E, Morillo J, Arnaiz C, Egea-Corbacho A, Usero J (2026) Bioremediation of contaminated soils with hydrocarbons using industrial wastewater treatment plant effluents in a circular economy model. ACS ES&T Water 6:3623–3633

Rittmann BE, McCarty PL (2001) Environmental biotechnology: principles and applications. McGraw-Hill, New York

Rončević S, Dalmacija B, Ivančev-Tumbas I, Tričković J, Petrović O, Klasnja M, Agbaba J (2005) Kinetics of degradation of hydrocarbons in the contaminated soil layer. Arch Environ Contam Toxicol 49:27–36

Ros M, Rodríguez I, García C, Hernández T (2010) Microbial communities involved in the bioremediation of an aged recalcitrant hydrocarbon-polluted soil using organic amendments. Bioresour Technol 101:6916–6923

Safdari M-S, Kariminia H-R, Rahmati M, Fazlollahi F, Polasko A, Mahendra S, Wilding WV, Fletcher TH (2018) Development of bioreactors for comparative study of natural attenuation, biostimulation, and bioaugmentation of petroleum-hydrocarbon contaminated soil. J Hazard Mater 342:270–278

Sarkar D, Ferguson M, Datta R, Birnbaum S (2005) Bioremediation of petroleum hydrocarbons in contaminated soils: comparison of biosolids addition, carbon supplementation, and monitored natural attenuation. Environ Pollut 136:187–195

Sayara T, Borràs E, Caminal G, Sarrà M, Sánchez A (2011) Bioremediation of PAHs-contaminated soil through composting: influence of bioaugmentation and biostimulation on contaminant biodegradation. Int Biodeterior Biodegrad 65:859–865

Scow KM, Simkins S, Alexander M (1986) Kinetics of mineralization of organic compounds at low concentrations in soil. Appl Environ Microbiol 51:1028–1035

Simkins S, Alexander M (1984) Models for mineralization kinetics with the variables of substrate concentration and population density. Appl Environ Microbiol 47:1299–1306

Smith MJ, Lethbridge G, Burns RG (1999) Fate of phenanthrene, pyrene and benzo[a]pyrene during biodegradation of crude oil added to two soils. FEMS Microbiol Lett 173:445–452

Suja F, Rahim F, Taha MR, Hambali N, Razali MR, Khalid A, Hamzah A (2014) Effects of local microbial bioaugmentation and biostimulation on the bioremediation of total petroleum hydrocarbons (TPH) in crude oil contaminated soil based on laboratory and field observations. Int Biodeterior Biodegrad 90:115–122

Taccari M, Milanovic V, Comitini F, Casucci C, Ciani M (2012) Effects of biostimulation and bioaugmentation on diesel removal and bacterial community. Int Biodeterior Biodegrad 66:39–46

Varjani SJ (2017) Microbial degradation of petroleum hydrocarbons. Bioresour Technol 223:277–286

Venzon DJ, Moolgavkar SH (1988) A method for computing profile-likelihood-based confidence intervals. J R Stat Soc Ser C Appl Stat 37:87–94

Wu M, Dick WA, Li W, Wang X, Yang Q, Wang T, Xu L, Zhang M, Chen L (2016) Bioaugmentation and biostimulation of hydrocarbon degradation and the microbial community in a petroleum-contaminated soil. Int Biodeterior Biodegrad 107:158–164

Yaman C (2020) Performance and kinetics of bioaugmentation, biostimulation, and natural attenuation processes for bioremediation of crude oil-contaminated soils. Processes 8:883. https://doi.org/10.3390/pr8080883

Supplementary Files

This is a list of supplementary files associated with this preprint. Click to download.

- YamanHMFOKMSupplementaryInformation.docx